Facile electrochemical synthesis of 3D nano-architectured CuO electrodes for high-performance supercapacitors

Journal:	*Journal of Materials Chemistry A*
Manuscript ID:	TA-ART-05-2014-002444
Article Type:	Paper
Date Submitted by the Author:	15-May-2014
Complete List of Authors:	Deng, Ming-Jay; National Synchrotron Radiation Research Center, Molecular Science Wang, Cheng-Chia; National Chiao Tung University, Department of Materials Science and Engineering Ho, Pei-Jung; National Hsinchu University of Education, Department of Applied Science Lin, Chih-Ming; National Hsinchu University of Education, Department of Applied Science Chen, Jin-Ming; National Synchrotron Radiation Research Center, Lu, Kueih-Tzu; National Synchrotron Radiation Research Center, Molecular Science

Journal Name

Dynamic Article Links ►

Cite this: DOI: 10.1039/c0xx00000x

www.rsc.org/xxxxxx

ARTICLE TYPE

Facile electrochemical synthesis of 3D nano-architectured CuO electrodes for high-performance supercapacitors

Ming-Jay Deng[a]†*, Cheng-Chia Wang[a,b]†, Pei-Jung Ho[a,c], Chih-Ming Lin[c], Jin-Ming Chen[a]*, Kueih-Tzu Lu[a]*

Received (in XXX, XXX) Xth XXXXXXXXX 20XX, Accepted Xth XXXXXXXXX 20XX

DOI: 10.1039/b000000x

With a simple electrochemical process, we prepared nano-architectured CuO electrodes with a 3D hierarchically porous structure and an excellent supercapacitive performance. These nano-architectured CuO electrodes were processed through the co-deposition of a Ni–Cu layer on Ni foam, selective etching of Cu from the Ni–Cu film (leaving tentacle-like nanoporous Ni), and anodic deposition of CuO nanoribbons (NR) on the tentacle-like nanoporous Ni/Ni foam substrate. Because of its unique nano-architecture, the prepared CuO nanoribbon-on-Ni-nanoporous/Ni foam (CNRNP) electrode shows exceptional performance of energy storage relative to a conventional version of the electrode. The CNRNP electrode has also a superior kinetic performance relative to a CuO nanoflake-on-Ni foam (CNFNF) and flake-like CuO (FLC) electrodes. Besides its excellent cyclic stability, an exceptionally large specific capacitance, 880 and 800 F g^{-1} (deducting substrates' capacitance from total), for the CNRNP electrode is obtained at scan rates 10 and 200 mV s^{-1}, respectively. The excellent pseudocapacitive characteristics of CNRNP electrodes associated with the variation of Cu oxidation state during charge and discharge cycles were elucidated with *in situ* X-ray absorption near-edge structure (XANES) spectra.

1 Introduction

The depletion of fossil fuels and the global warming require not only an urgent development of clean alternative energies and emission control of global warming gases, but also more effective systems for storage, conversion and management of energy. Supercapacitors (SC) have received considerable attention as a key device for energy storage because of their great power densities, rapid recharge capability and long cycle life;[1,2] they have thus become increasingly attractive for use in hybrid electric vehicles, consumer electronics, medical devices, and military missile systems. Pseudocapacitors, of which the capacitance is attributed mainly to the continuous and reversible redox reaction of electrode materials as an intermediate system between dielectric capacitors and batteries,[3,4] have attracted much interest because of their power density that exceeds that of secondary batteries, and energy density greater than that of typical carbonaceous materials with electric double-layer capacitors. To achieve a large capacitance, a pseudocapacitor normally combines non-faradaic electrostatic charge storage with redox reactions.[5-8] To improve the energy density of pseudocapacitors, much effort has been devoted to investigate pseudocapacitive transition-metal oxides, such as RuO_2, MnO_2, NiO, Co_3O_4.[5-15] RuO_2 is a material well known to have an ideal pseudocapacitive performance and a specific capacitance greater than 1000 F g^{-1},[9,10] but its great cost substantially limits its commercial application. Among these metal oxides, Cu oxide can be a promising candidate because of its low cost, abundance, non-toxicity and ease of preparation in diverse shapes of nanometre dimension, such as nanospheres, nanoflowers, nanorods and nanotubes. Besides supercapacitors, Cu oxides have served widely as electrode materials for catalysts and biosensors.[16,17] Cu-oxide nanostructures have been tested as anodes for Li-ion batteries and showed a large Li-ion storage capacity,[18] which indicates that Cu oxides can offer a large capacity for charge storage through a large redox activity, and great reversibility. The observed specific capacitance for Cu oxides is much smaller than for other transition-metal oxides, such as 1200 F g^{-1} for MnO_2 and 2200 F g^{-1} for Co_3O_4,[11,15] and it is still challenging and imperative to develop efficient but simple ways to enhance the utilization of electroactive Cu oxide, particularly at high rates.

The performance of SC is determined primarily by the electrochemical activity and kinetics of its electrodes. To improve the energy density of SC at high rates, it is hence critical to increase the transport rates of electrolyte ions and electrons in electrodes and at the interface between electrode and electrolyte, and to involve sufficient electroactive species exposed on the surface for the faradaic redox reaction.[19,20] The electrodes for electrochemical evaluation are generally enriched with binders produced with a slurry-coating technique, in which most electroactive surface of an electrode material becomes blocked from contact with an electrolyte.[13,14] Moreover, the polymer binder included markedly decreases the electrical conductivity of the electrode materials, then diminishing their performance. Scientists must thus ponder carefully how to design a suitable nano-architecture electrode that favors the penetration of electrolytes into the entire electrode matrix and at the same time decreases the electrical resistance in the electroactive materials and at the interface between the electrode material and the current collector.[13] Based on the above considerations, an ideal scheme is a nanoarray electrode free of binder, so self-supported, which is typically constructed with 1D or 2D building blocks and grown directly on the current collectors. An electrode of this type generally renders many advantages, such as effective electrical conductivity, small resistance to the diffusion of ionic species, ease of electrolyte penetration and a large electroactive area.[13,19,20] More precisely, in an electrode of this type, paths of both electrolyte ions and electrons are simultaneously constructed to enable an efficient energy storage at high rates, realizing a maximum application of electroactive material at a large current density.

Only little work has been performed on the application of CuO as a pseudocapacitor electrode because of its small electrical conductivity and unstable cycling performance.[21-23] The poor retention of capacitance upon cycling is due mainly to the destruction of the crystal structure of CuO during the ion insertion and extraction. A unique nano-architecture of the substrate material might alleviate this problem. Ni foam and Ni porous substrates improve the pseudocapacitive performance of electrodes.[13,24-28] A simple and scalable fabrication of 3D nano-architectured CuO for SC application has seldom been reported. Herein, we describe a facile synthesis of CuO nanoribbons (NR) on a tentacle-like nanoporous Ni/Ni foam to construct a 3D nano-architectured pseudocapacitive electrode with promising performance for charge storage. Ni foam is chosen as a substrate because of its large electrical conductivity and a desirable 3D porous structure. The preparation of a CuO nanoribbon-on-(tentacle-like)-Ni nanoporous/Ni foam (CNRNP) electrode is an entirely electrochemical process (Figure 1), which has the advantages of low cost, simplicity, versatility, accuracy and reliability.[29,30] The optimum specific capacitance (deducting substrates' capacitance from total) evaluated using cyclic voltammetry (CV), was as great as 880 F g^{-1} in KOH solution (3 M) at a potential scan rate 10 mV s^{-1} in a potential range –0.1 – +0.5 V (vs SCE). The cycling performance is acceptable, ~ 94 % retention after 5000 cycles. We compared the pseudocapacitive behavior of CuO nanoflake-on-Ni foam (CNFNF) and flake-like CuO (FLC) electrodes in KOH solution (3 M), respectively, and we elucidated the variation of the oxidation state of Cu of three electrodes in KOH solution using *in situ* X-ray absorption near-edge structure (XANES) spectra. This electrochemical capacitor exhibits an effective charge compensation in the Cu^+/Cu^{2+} reaction during rapid charge and discharge cycling with maximum variation ~0.85 of the Cu oxidation state. The CNRNP electrode exhibited a specific capacitance greater than that reported in the literatures.[21-23]

2 Experimental section

2.1 Apparatus and chemicals

All chemicals were of reagent quality and used without further purification. Ni–Cu alloy films were electrodeposited from a plating solution containing $NiSO_4$ (0.5 M), $NiCl_2$ (0.5 M), $CuSO_4$ (0.01 M), dimethyl sulfoxide (DMSO, 5 %) and H_3BO_3 (1 M, pH = 3.8). The deposition was performed at 27 ºC in a three-electrode cell with a Pt counter electrode and a saturated calomel reference electrode (SCE). Ni foam (area ~4.0 cm^2) was pretreated with degreasing in acetone, etching in hydrochloric acid, rinsing with water, soaking in $NiCl_2$ (0.01 M) for 6 h, and rinsing again thoroughly with water; after drying, the foam served as the working electrode so that adhesion was effective. The film was deposited under a constant potential –0.78 V; the total cathodic passed charge was controlled at 3 C cm^{-2}. Selective dissolution of Cu from the deposited alloy was then conducted in the same solution on applying an anodic potential 0.8 V until a terminal current density 10 μA cm^{-2} to develop the Ni nanoporous film, of density approximately 0.3 mg cm^{-2}.

2.2 Electrochemical Characterization.

The microstructure of the samples was examined with a scanning electron microscope (SEM, JEOL 6500F), X-ray energy dispersive spectroscope (EDS) and a transmission electron microscope (TEM, JEOL 2000F). The X-ray powder diffraction (XRD) of samples was performed at beamline BL01C2 of National Synchrotron Radiation Research Center (NSRRC), with x-rays of energy 18.0 keV (wavelength λ = 0.6888 Å); data collected with an image plate (Mar345) were calibrated with diffraction of mixed powders of silicon and silver behenate. For comparison, the synchrotron-based XRD patterns were converted to Cu Kα radiation. CuO was deposited anodically onto the nanoporous Ni substrate prepared in an alkaline solution bath containing $CuSO_4$ (0.1 M), $Cu(CH_3COO)_2$ (0.1 M) and tartaric acid (0.2 M), adjusted to pH ~9 on addition of NaOH (5 M). Tartaric acid acts as a stabilizer for Cu (II) ions to prevent its precipitation at pH higher than 7.[31,32] An anodic potential 0.6 V (vs. SCE) was applied to yield a total passed charge density 0.4 C cm^{-2}. The typical mass densities, measured with a microbalance of accuracy 0.01 mg, of the deposited CuO was approximately 0.32 mg cm^{-2}. The nanostructured electrode obtained was examined with a SEM. The same amount of CuO was deposited on a Ni foam and flat Ni substrate to make counterpart electrodes. The flat Ni (area ~4.0 cm^2) was pretreated on degreasing in acetone, etching in hydrochloric acid, and rinsing thoroughly with water; after drying it served as the working electrode. The electrochemical performance of the three electrodes was evaluated with cyclic voltammetry (CV) in KOH solution (3 M) at 27 ºC; the potential was scanned in a range –0.1 – +0.5 V (vs. SCE) with varied sweep rates (10 – 200 mV s^{-1}). Electrochemical impedance spectra (EIS) were recorded on applying an AC voltage of amplitude 5 mV s^{-1} in a frequency range from 0.01 Hz to 100 kHz at the open-circuit potential. The applied potential and current were regulated with a potentiostat (Autolab). The variation of the oxidation state of Cu in the CNRNP electrode was investigated at various applied potentials in KOH solution (3 M) with *in situ* Cu K-edge XANES spectra recorded in the fluorescence-yield mode. A sealed spectro-electrochemical cell with a fluorescence-transparent Kapton tape window was used. Before measuring the absorption spectra at a given potential, we maintained the electrode at a set potential for 10 min to allow the CNRNP electrode to attain a steady state. The *in situ* Cu K-edge XANES measurements were conducted at beamlines BL01C1 and BL17C1 of NSRRC. A Si(111) double crystal monochromator served to tune the X-ray photon energy with resolution $\Delta E/E$ ~2 × 10^{-4}. The X-ray absorption energy was calibrated with the known Cu K-edge absorption inflection point at 8978.9 eV of a Cu foil, which was measured before each XANES scan. X-ray photoemission spectroscopy (XPS) were used to probe the oxidation state of Cu at beamline BL20A of NSRRC.

3 Results and discussion

Our research strategy is illustrated in Figure 1. Figure S1† shows the CV of a blank Ni foam electrode recorded in the plating solution ($NiSO_4$ 0.5 M, $NiCl_2$ 0.5 M, $CuSO_4$ 0.01 M, DMSO 5 %, H_3BO_3 1 M). Through a potential scan of the electrode from the open-circuit potential (0.13 V) in a negative direction, the onset of the Cu reduction current at approximately 0.1 V was followed by a reduction signal associated with the nucleation and growth of Cu. As Cu(II) has a limited mass transfer because of its small concentration, the deposition current varied insignificantly with potential until –0.6 V, at which point Ni(II) reduction began. At a more negative potential, Ni and Cu were co-deposited. The anodic signals about 0.8 V are attributed to a selective dissolution of Cu from the Ni–Cu layer in the deposit. To elucidate the reaction mechanism, we used SEM, XRD, XANES and XPS to examine the chemical and physical properties of the deposits.

According to Figure S1†, the co-deposition of a Ni–Cu layer and then the selective etching of Cu from the deposit was completed in the same solution on simply switching the applied potential (at –0.78 V and +0.8 V, respectively). Figure 2 (a) shows the granular morphology of the film deposited at –0.78 V, which had a Ni/Cu atomic ratio approximately 45/55 (confirmed with EDS). As shown in Figure 2 (a), during the deposition, new grains seemed to form on preceding ones, growing into a protruding structure; they tended to overlap and to aggregate into clusters while the passed charge was increased. Figure 2 (b) shows a SEM image of the tentacle-like Ni nanoporous film after being etched at 0.8 V. While the clustering of the Ni–Cu grains led to formation of connected pores upon etching (less than 2 at. % of residual Cu was found), the morphology gradually became a tentacle-like Ni nanoporous structure remaining through its passivation. The pore size was in a range 30 – 90 nm; the pore density was about 10^{13} cm^{-2}. The comparison of the deposition potential on the morphology is illustrated in Figure S2†, which shows the plane view SEM micrographs for Ni-Cu films after complete electrochemical etching at 0.8 V. Figure 2a† shows that etching a Ni-Cu film deposited at -0.70V (Ni/Cu atomic ratio approximately 30/70 (confirmed with EDS)) results in the formation of pores 150-250 nm in diameter but the density of the pores is small. Figure S2b† shows that etching the Ni-Cu film deposited at -0.85 V (Ni/Cu atomic ratio approximately 65/35) results in carrot-like deposits with tiny holes on their central parts. Figure 2 (c) shows an image of the tentacle-like Ni film (thickness about 5 μm) at less magnification. The tentacle-like Ni nanoporous film of great density was observed to grow uniformly on the skeleton of the Ni foam, forming a 3D hierarchical structure (inset in Figure 2 (c)). In contrast to the flat Ni substrate used, the Ni foam had a much more effective adhesion to the nanoporous Ni film. As a thicker film was allowed, a 3D hierarchically porous structure was available. Figure 2 (c) shows that a highly porous structure was found throughout the layer. This observation confirms that the Ni–Cu film as deposited on the Ni foam consisted of numerous interconnected Ni–Cu particles, and that the layer underneath was still etching electrolyte accessible because of the high porosity. Figure 2 (d) shows the XRD patterns of the Ni–Cu film before and after etching at 0.8 V, revealing that the Cu-rich phase was selectively removed. Figure 2 (e) shows the Cu $2p_{3/2}$ XPS spectra recorded from the film deposited at –0.78 V. The binding-energy signal at 932.7 eV corresponds to Cu at zero valence.[33] After etching, the corresponding XPS spectra are also shown in Figure 2 (e); the intensity of the Cu $2p_{3/2}$ signal decreased significantly after etching. The results clearly confirm that, through the formation of a surface-oxide layer in the sulfate solution, Ni became passivated and remained on the electrode while Cu was selectively removed under the anodic applied potential. The results presented in Figure 2 indicate that the central part of each grain was a Cu-rich region that was favorably dissolved when an anodic potential was applied, which created the tentacle-like Ni nanostructures. Chemical segregation within deposited Ni–Cu grains was observed by previous authors.[26,27] We have thus developed an efficient electrochemical technique to construct 3D hierarchical Ni porous/Ni foam substrates. The feature size of the nanoarchitectures obtained was smaller than those of the existing Ni foam and flat Ni substrates used for pseudocapacitors;[13,24,25] enhancement of the performance of an electroactive material is hence to be expected. The remaining tentacle-like Ni nanoporous/Ni foam with 3D nano-porosity was then used to load the CuO NR.

To attain an entirely electrochemical procedure for fabrication of a 3D hierarchically porous CuO capacitor electrode, we attempted direct electrodeposition of CuO NR on the prepared tentacle-like Ni porous/Ni foam substrates. Figure 3 (a) shows the morphology of the anodically deposited CuO NR on the prepared tentacle-like Ni porous/Ni foam template. CuO NR of width only a few nanometers was observed to be uniformly distributed on the nanosize Ni tentacles, even inside the pores, forming a 3D micro-meso-macro-porous structure. This result proves that a 3D nano-architecture CuO electrode with great surface area and a hierarchically porous structure was implemented. The crystal structure and phase purity of the CuO products were analyzed with XRD, as shown in Figure 3 (b). All identified diffraction signals were matched satisfactorily with the standard pattern of monoclinic CuO (JCPDS card No. 05-661).[34] No signal from possible impurities such as Cu, $Cu(OH)_2$, or Cu_2O was detected. A typical TEM image of CuO NR appears in Figure 3(c); the inset that shows the SAED pattern of CuO NR as prepared indicates that the ribbons were well crystallized. The diffraction rings on the SAED image match the features in the XRD pattern, which proves also the monoclinic structure of CuO NR as prepared. Figure 3(d) presents the Cu $2p_{3/2}$ XPS spectrum recorded from the electrode shown in Figure 3 (a). The existence of *shake-up* satellites in the Cu 2p signal eliminates the presence of Cu^{2+}. The Cu $2p_{3/2}$ photoemission signal fits perfectly with a line centered at binding energy 933.6±0.1 eV, as shown in Figure 3(d). This analytical result confirms that the electrochemically prepared electrodes are CuO.[35] Figure 3(e) and (f) show the morphologies of the prepared Cu oxide electrodes with flat Ni and Ni foam substrates, respectively. On the flat Ni substrate, massive flake-like CuO (FLC) was observed above a granular but compact lower layer. On the Ni foam substrate, CuO nanoflakes (CNFNF) were observed to form a thick, uniform film, which completely covered the Ni foam framework. The Brunauer-Emmett-Teller (BET) surface areas of these samples were determined to be 50.6 m^2 g^{-1} for the FLC electrode, 94.8 m^2 g^{-1} for the CNFNF electrode and 196.1 m^2 g^{-1} for the CNRNP electrode. About 78% of the total pore volume of the CNRNP electrode was contributed by pores under 50 nm. The corresponding density functional theory (DFT) pore size distribution of the CNRNP electrode exhibits a hierarchical pore structure that includes micro- (< 2 nm, 17%)., meso- (2–50 nm, 61%), and macropores (> 50 nm, 22%). However, about 30 and 55% of the total pore volume of the CNFNF and FLC electrode were contributed by pores under 50 nm, respectively. The BET test was done by testing the whole synthesized structure and then minus the blank substrates (Ni foam or flat Ni). The significantly increased surface area was due to the highly ordered tentacle-like porous structures, consistent with the observation from the SEM images shown in Figure 2 and 3. We applied directly the CNRNP, CNFNF and FLC as electrodes for SC to compare the merits of the unique architecture. The electrochemical tests were performed in a three-electrode configuration with a Pt counter electrode and a SCE in an aqueous electrolyte (KOH 3 M). The pseudocapacitive characteristic of each electrode was then systematically evaluated, as discussed in the following sections.

Figure 4 (a) shows the CV of the CNRNP, CNFNF and FLC electrodes at a scan rate 10 mV s^{-1}. For each curve, a symmetric pair of anodic and cathodic peaks over the entire range of scan rates was clearly observed, which reveals that the capacitive characteristic was distinct from that of the electric double-layer capacitance of which the CV curves have a nearly rectangular shape. The result indicates clearly that reversible and continuous faradaic reactions of Cu oxide were involved during the electrode charging and discharging. The pseudocapacitance of the Cu oxide electrode is a result of transitions between oxidation state Cu(I) and Cu(II) in the oxide, and vice versa. This redox reaction for the Cu oxide electrode is proposed:

$$CuO + 1/2\, H_2O + e^- \longleftrightarrow 1/2\, Cu_2O + OH^- \quad (1)$$

The redox signals appearing for samples in KOH solution are attributed to the oxidation of Cu_2O to CuO and back to Cu_2O (Eq. (1)). In Figure 4 (a), the CV curve enclosed area, which corresponds to the energy storage capability, increases with increasing surface area. The CV curve of a bare porous Ni electrode measured under the same conditions is superimposed in Figure 4(a). As little Ni oxide was formed (on passivation) on the electrode surface, the current is much smaller than that of the 3D nano-architecture Cu oxide electrodes. The specific capacitance (C) of CuO on various substrates was quantitatively evaluated according to the following equation,

$$C = Q_m / \Delta V \qquad (2)$$

in which Q_m denotes the specific voltammetric charge (based on the mass of CuO) integrated from the CV curve, and ΔV denotes the potential scanning range (i.e. 0.6 V ×2). The calculated capacitances (deducting substrates' capacitance from total) of the CNRNP and CNFNF electrodes are 880 and 450 F g^{-1}, respectively. In contrast, the FLC on a flat Ni substrate displays a capacitance only 200 F g^{-1}, which is larger than what is typically reported for commercial CuO powder and a CuO thin film.[21-23] Figure 4 (b) presents the CV curves of the CNRNP electrode recorded at varied potential scan rates. The symmetric characteristic, according to which the anodic and cathodic charges are almost the same, was maintained even at a high scan rate. The response current of the electrode, increasing quasi-linearly with the potential scan rate, revealed its excellent reactivity and reversibility. The optimum specific capacitance (C_{sp}) of the CNRNP electrode evaluated at 200 mV s^{-1} is 800 F g^{-1}; i.e. as much as 91 % of the capacitance was maintained relative to that measured at 10 mV s^{-1}, as shown in Figure 4 (c). In contrast, the CNFNF and FLC electrodes reserved only 81 and 69 % of initial C_{sp} when the potential scan rate was increased by the same extent, respectively. This specific capacitance and high-rate capability outperforms any existing Cu-oxide electrodes reported in the literatures.[21-23] Plots of galvanostatic charge−discharge voltage vs. time of CNRNP electrodes were measured at an applied potential from –0.1 V to +0.5 V, as shown in Figure 4 (d). A symmetric triangular shape with well defined plateaus during the charges-discharge processes was observed, indicating their satisfactory pseudo-capacitive behavior. With the rate of charging and discharging increased from 1.5 to 20 A g^{-1}, the CNRNP electrode showed a C_{sp} loss only ~24 %, which is much smaller than that, over 40 %, of the CNFNF and FLC electrodes, indicating a superior rate capability of the CNRNP electrodes. The specific capacitance of CuO was measured also with chronopotentiometry according to

$$C = I\, \Delta t / \Delta V\, w \qquad (3)$$

in which I is the applied current (1.5 A g^{-1}), ΔV is the potential scan range (i.e. 0.6 V ×2), Δt is the duration of a charge–discharge cycle, and w is the mass of CuO. C_{sp} was as large as 900 F g^{-1}, which is near that estimated from the CV, again confirming the extraordinary capacity for charge storage. To confirm the influence of the 3D nano-architecture on the electrochemical performance, we show electrochemical impedance spectra (EIS) in Figure S3†. The impedances of the three electrodes all consist of a depressed arc in the region of large frequency and a linear slope at small frequency. The semicircle reflects the electrochemical reaction impedance of the film electrode; the straight line indicates the diffusion of the electroactive species. The CNRNP electrode exhibits a smaller capacitive arc and a smaller slope than the CNFNF and FLC electrodes. A larger semicircle is accepted to imply a larger charge-transfer resistance, and a larger slope signifies more rapid diffusion. We conclude that the CNRNP electrode has the least charge-transfer resistance and ion-diffusion resistance, corresponding to a much increased conductivity, which is beneficial for the rate capability of the unique structure. The significant differences of the current intensity and superior performance between the CNRNP, CNFNF and FLC electrodes in Figure 4 are attributed to the unique 3D hierarchical structure. In particular, the tentacle-like Ni nanoporous/Ni foam substrate with nano/micro-scale voids and the flow channels that follow a zigzag path give the electrode an efficient mass transport and a great ratio of effective surface area. Each CuO NR is connected directly to the tentacle-like Ni nanoporous/Ni foam skeleton with effective mechanical adhesion, which not only generates a path for rapid electron transport and minimizes the interface resistance, but also removes the need for binders and conductive additives required in a typical electrode. The greatly dispersed CuO NR further increases the contact area between electrolyte and electrode and facilitates rapid ion diffusion, thus enhancing the electrochemical kinetics. The open micro-meso-macro-porous structure between nanoribbons serves as an *ion-buffering pool* of OH^- ions,[13] which confirms that sufficient faradaic reaction can occur even at large current densities. This effect also indicates that a large C_{sp} is still achievable at a large current density with an appropriately designed 3D conductive electrode framework. The large specific capacitance can decrease the amount of oxide (thus the prime cost) used for a capacitor, preserving natural resources. Figure S4† demonstrates the capacitance retention ratios as a function of CV scan rate for various electrodes that we prepared. The CNRNP electrodes clearly show a superior high-rate performance superior to that of the CNFNF and FLC electrodes. For example, with a CuO deposition amount 0.32 mg cm^{-2}, the electrode with the tentacle-like nanoporous Ni/Ni foam substrate retained over 90 % capacitance when the potential scan rate was increased from 10 to 200 mV s^{-1} whereas the counterpart electrodes retained only 81 and 69 % of initial C_{sp} under the same conditions. When the CuO loading was increased to 1.2 mg cm^{-2}, a satisfactory capacitance retention ratio 82 % was still achieved for the CNRNP' electrode when the CV scan rate increased from 10 to 200 mV s^{-1}, but much smaller values 70 % and 52 %, respectively, were found for the CNFNF' and FLC' electrodes because of their kinetic limitation. The electrochemical stability of the electrodes was evaluated on repeating the charge-discharge cycles. The CNFNF and FLC electrodes suffered capacitance decays 30 % and 42 % after 5000 charge–discharge cycles, respectively. AAS analytical data revealed that only 70 % and 58 %, respectively, of the initial CuO remained after the cycling, indicating that the capacitance fading was attributed mainly to the loss of the active material. In contrast, the CNRNP electrode suffered a capacitance decay 6 % after 5000 charge–discharge cycles (see ESI Figure S5†); according to AAS analyses, more than 94 % of the CuO remained on the electrode. These results further signify the exceptional capability of this unique tentacle-like nanoporous Ni/Ni foam-supported CuO NR electrode to meet the requirements for both large C_{sp} and a long cycle life, which are essential characteristics for high-performance devices for energy storage. To confirm this proposition, we investigated the pseudocapacitive characteristics of these electrodes *in situ* in the KOH solution with XANES spectra.

Figure 5(a) shows *in situ* Cu K-edge XANES spectra of the CNRNP electrode measured under five applied potentials in a sequence −0.1 V, +0.2 V then +0.5 V and +0.2 V finally −0.1 V. The adsorption rising edge of the Cu K-edge spectra of the CNRNP electrode shifted toward greater energy with increasing applied potential, and returned nearly to the initial position when the potential was reversed. The absorption threshold energy (E_0), which is obtained from the first inflection point on the absorption edge, is linearly correlated with the oxidation state of a transition metal in materials.[36] Based on E_0 derived from the X-ray absorption spectra in Figure 5(a), the average oxidation state of Cu of the CNRNP electrode in KOH solution was determined in the sequence shown in Figure 5(b). (Reference samples such as Cu, Cu_2O(I) and CuO(II) were also analyzed; the corresponding E0 were 8978.9, 8980.4 and 8983.6 eV, respectively.)[36] Figure 5(b) shows also the average oxidation state and *in situ* Cu K-edge XANES spectra of the CNFNF electrode in a sequence −0.1 V, then +0.5 V and finally −0.1 V, and the FLC electrode in a sequence −0.1 V, then +0.5 V and finally −0.1 V, respectively, both in KOH solution. In addition, the incomplete recovery of the Cu oxidation state (from +1.09 to +1.11) after the electrochemical redox cycle was considered to be a reason for the decay of capacitance of the oxide electrode during charge and discharge. The variation of the Cu oxidation state between −0.1 V and +0.5 V with a CNRNP electrode is approximately 0.85, which is greater than that with the CNFNF and FLC electrodes. The results confirm that the highly porous nanostructure minimizes the distances of both ionic and electronic transport in the CNRNP and thus improves the electrode kinetic performance, contributing to the significant capacitance observed in Figure 4, which is a crucial concern for a high-performance supercapacitor.

Conclusions

A facile, inexpensive and potentially scalable technique has been developed to fabricate well designed Cu NR on a tentacle-like nanoporous Ni/Ni foam for high-performance SC. The synthesis involves the co-deposition of a Ni–Cu layer on the Ni foam, selective etching of Cu from the Ni–Cu film (leaving tentacle-like nanoporous Ni), and anodic deposition of CuO NR on the tentacle-like nanoporous Ni/Ni foam substrate. Because of its unique 3D nano-architecture, the prepared CuO NR-on-Ni nanoporous/Ni foam electrode endows rapid ion and electron transport, a large electroactive surface area and excellent structural stability. As a result, the CNRNP electrode exhibits an exceptional pseudocapacitance, as great as 880 F g^{-1}, and an outstanding rapid redox capability, relative to those of the CNFNF and FLC electrodes. The unique 3D nano-architectured substrate preserves an active material-cycling stability up to 5000 cycles. The proposed fabrication of 3D nano-architectured electrodes is expected to be applicable to the loading of other electroactive materials to improve their sensing, catalytic and energy-storage performances.

Acknowledgements

We thank the NSRRC staff for their technical support. This research is supported by the NSRRC and the National Science Council of the Republic of China under grant numbers NSC 99-2113-M-213-007 and 102-2113-M-213-004

Inserting Graphics

Notes and references

a National Synchrotron Radiation Research Center, Hsinchu, Taiwan. Fax: +886-3-578-3813; Tel: +886-3-578-0281; E-mail: deng.mj@nsrrc.org.tw; martinez730523@yahoo.com.tw; jmchen@nsrrc.org.tw; ktlu@nsrrc.org.tw
b Department of Materials Science and Engineering, National Chiao Tung University, Hsinchu, Taiwan
c Department of Applied Science, National Hsinchu University of Education, Hsinchu, Taiwan

† Electronic Supplementary Information (ESI) available: [details of any supplementary information available should be included here]. See DOI: 10.1039/b000000x/

References

1. *Electrochemical Supercapacitors*, ed. B. E. Conway, Kluwer-Plenum, New York, 1999.
2. P. Simon and Y. Gogotsi, *Nat. Mater.*, 2008, **7**, 845.
3. T. Brezesinski, J. Wang, S. H. Tolbert and B. Dunn, *Nat. Mater.*, 2010, **9**, 146.
4. Y. Hou, Y. W. Cheng, T. Hobson and J. Liu, *Nano Lett.*, 2010, **10**, 2727.
5. Y. S. Shim and H. J. Kim, *ACS Nano*, 2010, **4**, 2345.
6. M. B. Sassin, A. N. Mansour, K. A. Pettigrew, D. R. Rolison and J.W. Long, *ACS Nano*, 2010, **4**, 4505.
7. S. W. Lee, J. Y. Kim, S. Chen, P. T. Hammond and Y. S. Horn, *ACS Nano*, 2010, **4**, 3889.
8. B. Balasubramanian, K. L. Kraemer, N. A. Reding, R. Skomski, S. Ducharme and D. J. Sellmyer, *ACS Nano*, 2010, **4**, 1893.
9. K. H. Chang, C. C. Hu and C. Y. Chou, *Chem. Mater.*, 2007, **19**, 2112.
10. C. C. Hu, K. H. Chang, M. C. Lin and Y. T. Wu, *Nano Lett.*, 2006, **6**, 2690.
11. Q. Li, Z. Wang, G. Li, R. Guo, L. Ding and Y. Tong, *Nano Lett.*, 2012, **12**, 3803.
12. M. J. Deng, P. J. Ho, C. Z. Song, S. A. Chen, J. F. Lee, J. M. Chen and K. T. Lu, *Energy Environ. Sci.*, 2013, **6**, 2178.
13. C. Yuan, L. Yang, L. Hou, L. Shen, X. Zhang and X. W. Lou, *Energy Environ. Sci.*, 2012, **5**, 7883.
14. B. Wang, T. Zhu, H. B. Wu, R. Xu, J. S. Chen and X. W. Lou, *Nanoscale*, 2012, **4**, 2145.
15. M. J. Deng, F. L. Huang, I. W. Sun, W. T. Tsai and J. K. Chang, *Nanotechnology*, 2009, **20**, 175602.
16. X. H. Xia, J. P. Tu, X. L. Wang, C. D. Gu and X. B. Zhao, *Chem. Commun.*, 2011, **47**, 5786
17. X. H. Xia, J. P. Tu, Y. J. Mai, X. L. Wang, C. D. Gu and X. B. Zhao, *J. Mater. Chem.*, 2011, **21**, 9319.
18. M. F. Cain, R. P. Hughes, D. S. Glueck, J. A. Golen, C. E. Moore and A. L. Rheingold, *Inorg. Chem.*, 2010, **49**, 7650.
19. R. K. Bedi and I. Singh, *ACS Appl. Mater. Interfaces*, 2010, **2**, 1361.
20. J. C. Park, J. Kim, H. Kwon, H. Song, *Adv. Mater.*, 2009, **21**, 803.
21. D. P. Dubal, D. S. Dhawale, R. R. Salunkhe, V. S. Jamdade, C. D. Lokhande, *J. Alloys Compd.*, 2010, **492**, 26.
22. Y. Hsu, Y. Chen and Y. Lin, *J. Electroanal. Chem.*., 2012, **673**, 43.
23. D. Kim, K. Rhee and S. Park, *J. Alloy. Compd*., 2012, **530**, 6.
24. M. J. Deng, J. K. Chang, C. C. Wang, K. W. Chen, C. M. Lin, M. T. Tang, J. M. Chen and K. T. Lu, *Energy Environ. Sci.*, 2011, **4**, 3942.
25. G. W. Yang, C. L. Xu and H. L. Li, *Chem. Commun.*, 2008, 6537.
26. L. Sun, C. L. Chien and P. C. Searson, *Chem. Mater.*, 2004, **16**, 3125.
27. Z. Liu, D. Elbert, C. L. Chien and P. C. Searson, *Nano Lett.*, 2008, **8**, 2166.
28. J. K. Chang, S. H. Hsu, W. T. Tsai and I. W. Sun, *J. Power Sources*, 2008, **177**, 676.
29. G. S. Attard, P. N. Bartlett, N. R. B. Coleman, J. M. Elliott, J. R. Owen and J. H. Wang, *Science*, 1997, **278**, 838.
30. P. A. Nelson, J. M. Elliott, G. S. Attard and J. R. Owen, *Chem. Mater.*, 2002, **14**, 524.
31. P. Poizot, C. Hung, M. P. Nikiforov, E. W. Bohannan and J. A. Switzer, *Electrochem. Solid-State Lett.*, 2003, **6**, C21.
32. H. M. Kothari, E. A. Kulp, S. Boonsalee, M. P. Nikiforov, E. W. Bohannan, P. Poizot, S. Nakanishi and J. A. Switzer, *Chem. Mater.*, 2004, **16**, 4232.
33. P. Marcus and M. E. Bussell, *Appl. Surf. Sci.*, 1992, **59**, 7.
34. M. Vaseem, A. Umar, S.H. Kim, Y.B. Hahn, *J. Phys. Chem. C*, 2008, **112**, 5729.
35. M. C. Biesinger, L.W.M. Lau, A. R.Gerson and R. S. C. Smart, *Appl. Surf. Sci.*, 2010, **257**, 887.
36. S. Bijani, M. Gabas, G. Subias, J. Garcia, L. Sanchez, J. Morales, L. Martineza and J. R. Ramos-Barrado, *J. Mater. Chem.*, 2011, **21**, 5368.

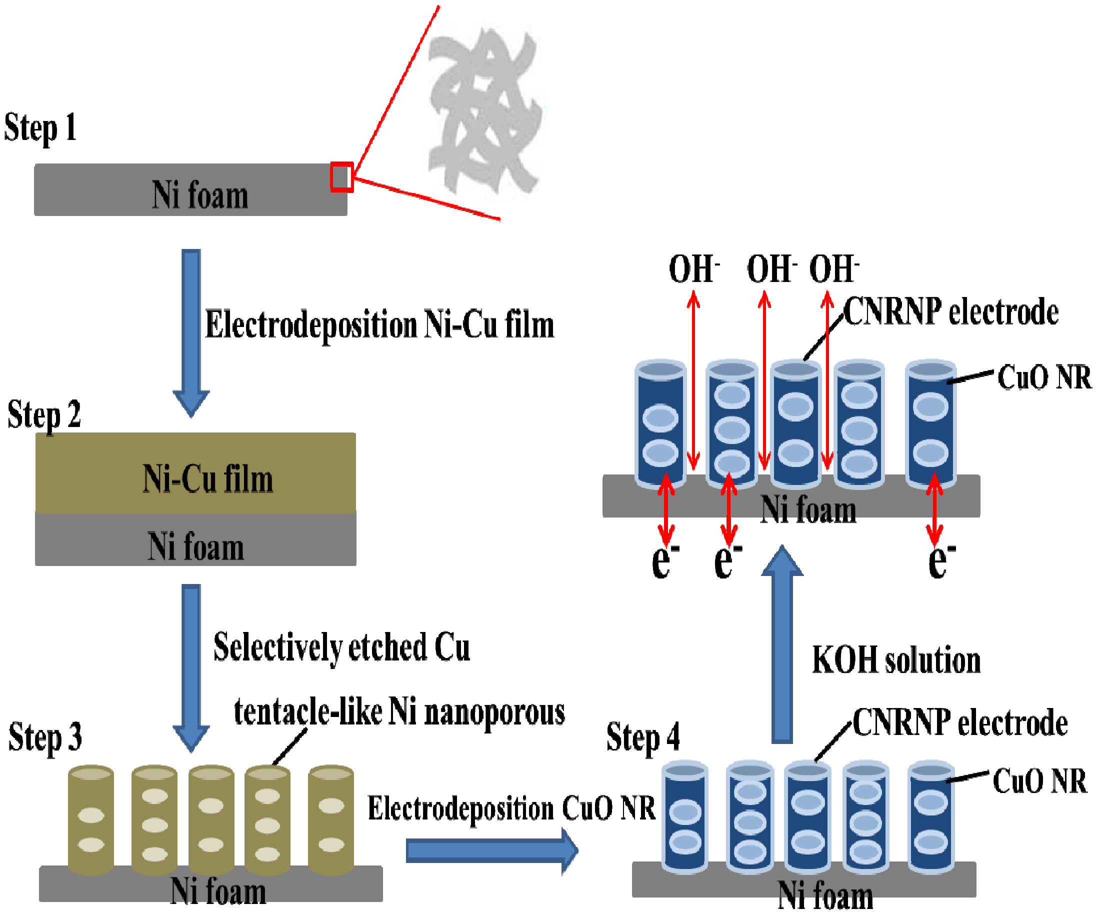

Figure 1. Scheme of electrochemical preparation of a highly porous CNRNP electrode.

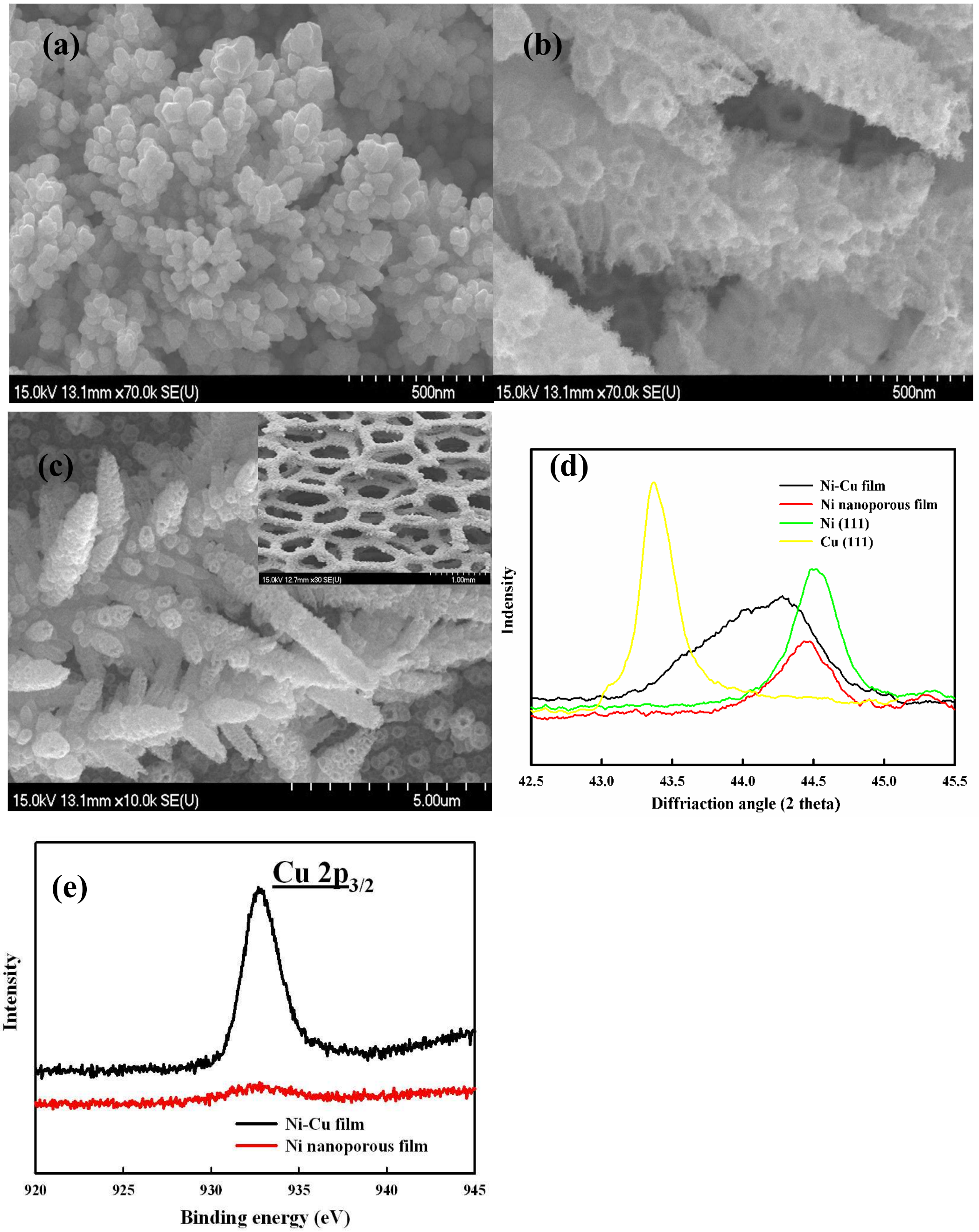
(a)
15.0kV 13.1mm x70.0k SE(U)
500nm
(b)
15.0kV 13.1mm x70.0k SE(U)
500nm
(c)
15.0kV 12.7mm x30 SE(U)
1.00mm
15.0kV 13.1mm x10.0k SE(U)
5.00um
(d)
Ni-Cu film
Ni nanoporous film
Ni (111)
Cu (111)
Indensity
42.5
43.0
43.5
44.0
44.5
45.0
45.5
Diffriaction angle (2 theta)
(e)
Cu 2p3/2
Intensity
Ni-Cu film
Ni nanoporous film
920
925
930
935
940
945
Binding energy (eV)

Figure 2 (a) SEM micrographs of the Ni-Cu alloy films as deposited on Ni foam obtained on constant potential electrodeposition at –0.78 V. (b) The nanoporous Ni film after Cu was selectively etched. (c) Image of the nanoporous Ni at a smaller magnification and (d) X-ray diffraction patterns for Ni–Cu films deposited before and after etching the Cu. (e) Cu $2p_{3/2}$ XPS spectra recorded from the Ni-Cu film as deposited at –0.78 V, and the film etched at 0.8 V. The electrodeposition and selective dissolution were performed in solution ($NiSO_4$ 0.5 M, $NiCl_2$ 0.5 M, $CuSO_4$ 0.01 M , DMSO 5 %, H_3BO_3 1 M).

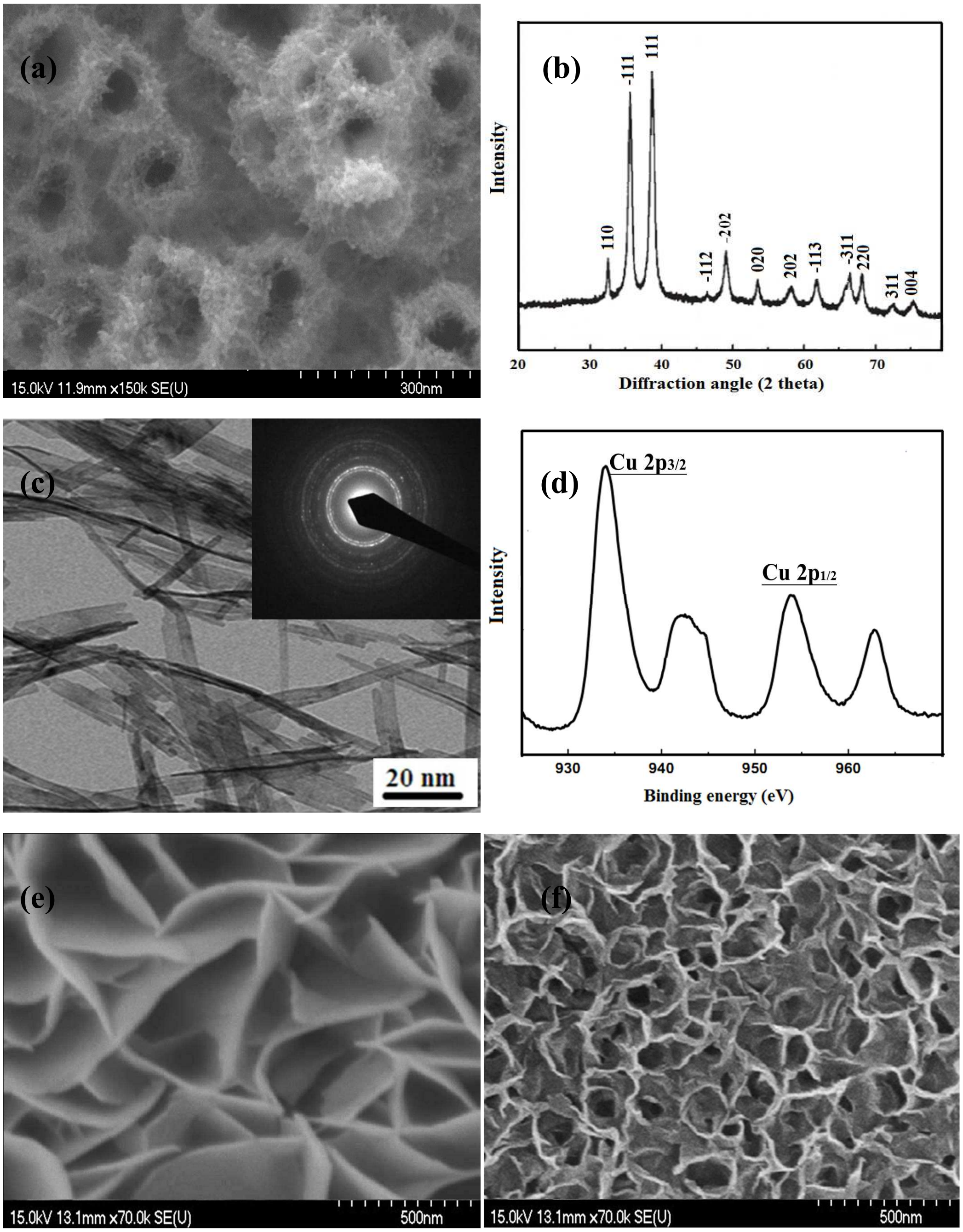
(a)
15.0kV 11.9mm x150k SE(U)
300nm
(b)
Intensity
-111
111
110
-202
-112
020
202
-113
-311
220
311
004
20
30
40
50
60
70
Diffraction angle (2 theta)
(c)
20 nm
(d)
Cu 2p3/2
Cu 2p1/2
Intensity
930
940
950
960
Binding energy (eV)
(e)
15.0kV 13.1mm x70.0k SE(U)
500nm
(f)
15.0kV 13.1mm x70.0k SE(U)
500nm

Figure 3 (a) High-resolution SEM micrographs of the CuO NR electrodes prepared with the Ni porous substrate; (b) X-ray diffraction patterns for CuO NR films; (c) TEM image of CuO NR structure. The inset shows the SAED pattern of CuO NR as prepared. (d) Cu 2p XPS spectra of the CuO NR film. SEM micrographs of the CuO electrodes prepared on (e) the flat Ni substrate and (f) the Ni-foam substrate.

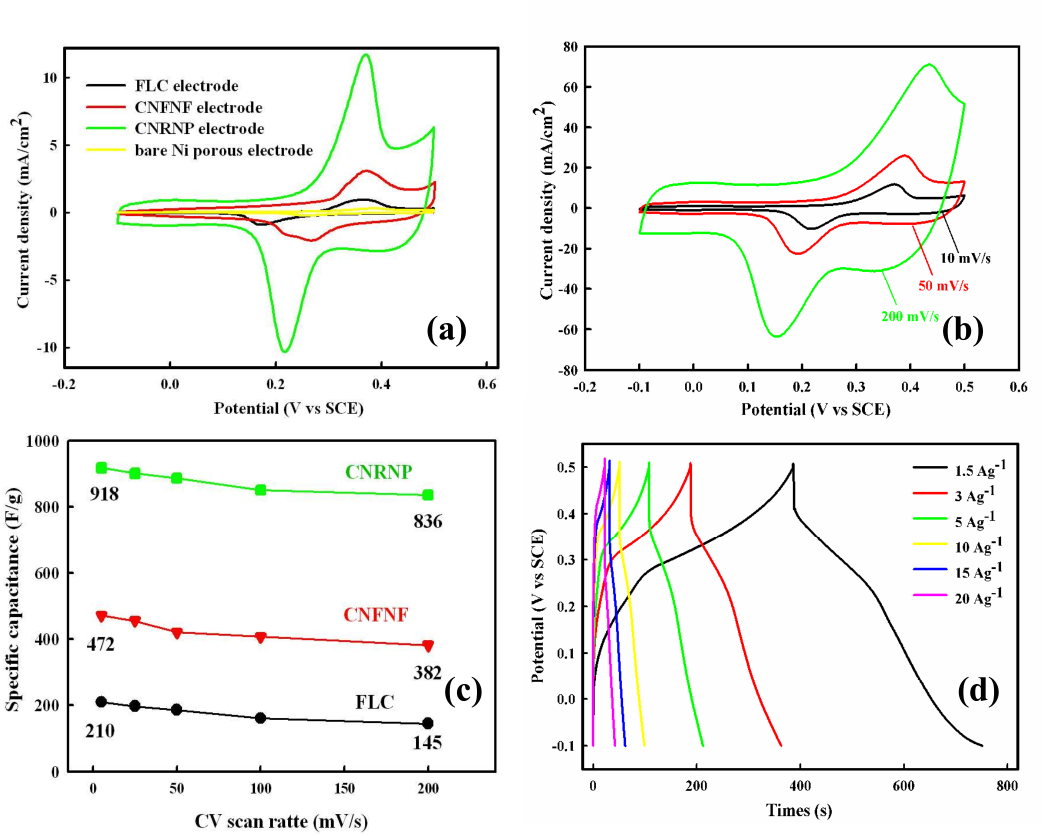

Figure 4 (a) Cyclic voltammograms of CNRNP, CNFNF and FLC electrodes recorded in solution (KOH 3 M) at a potential sweep rate 10 mV s^{-1}; (b) cyclic voltammograms of the CNRNP electrode at various scan rates (10 – 200 mV s^{-1}); (c) specific capacitance of the CNRNP, CNFNF and FLC electrodes recorded at various potential scan rates relative to that measured at 10 mV s^{-1} (CuO deposition amount 0.32 mg cm^{-2}); (d) **c**harge–discharge curves of the CNRNP electrode measured in the potential range from −0.1 V to +0.5 V at varied current densities (1.5–20 A g^{-1}).

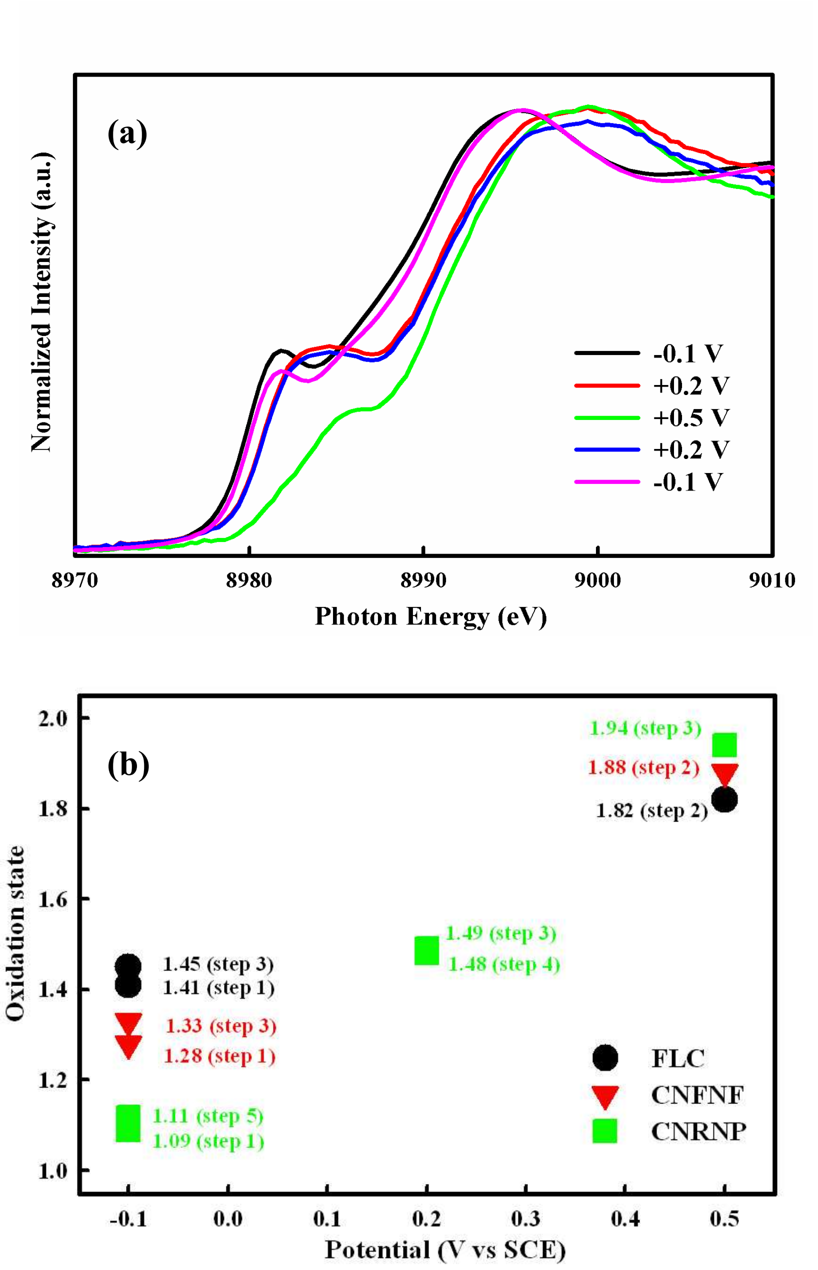

Figure 5 (a) *in situ* Cu K-edge XANES spectra of the CNRNP electrode measured in KOH solution (KOH 3 M) under various applied potentials. (b) Variation of Cu oxidation state in KOH solution with various applied potentials.